Whole-Body Image Registration Using Patient-Specific Non-Linear Finite Element Model

Mao Li[a], Adam Wittek[a], Grand Joldes[a], Guiyong Zhang[a], Feifei Dong[b], Ron Kikinis[c] and Karol Miller[a]

[a]Intelligent Systems for Medicine Laboratory,

The University of Western Australia, Perth, Australia

[b]Chengdu Monitoring Station,

The State Radio Monitoring Centre, Chengdu, China

[c]Surgical Planning Laboratory,

Brigham and Women's Hospital, Harvard Medical School, Boston, MA, USA

Abstract Registration of whole-body radiographic images is an important task in analysis of the disease progression and assessment of responses to therapies. Numerous registration algorithms have been successfully used in applications where differences between source and target images are relatively small. However, registration of whole-body CT scans remains extremely challenging for such algorithms as it requires taking large deformations of body organs and articulated skeletal motions into account. For registration problems involving large differences between source and target images, registration using biomechanical models has been recommended in the literature. Therefore, in this study, we propose a patient-specific non-linear finite element model to predict the movements and deformations of body organs for the whole-body CT image registration. We conducted a verification example in which a patient-specific torso model was implemented using a suite of non-linear finite element algorithms we previously developed, verified and successfully used in neuroimaging registration. When defining the patient-specific geometry for the generation of computational grid for our model, we abandoned the time-consuming hard segmentation of radiographic images typically used in patient-specific biomechanical modelling to divide the body into non-overlapping constituents with different material properties. Instead, an automated Fuzzy C-Means (FCM) algorithm for tissue classification was applied to assign the constitutive properties at finite element mesh integration points. The loading was defined as a prescribed displacement of the vertebrae (treated as articulated rigid bodies) between the two CT images. Contours of the abdominal organs obtained by warping the source image using the deformation field within the body predicted using our patient-specific finite element model differed by only up to only two voxels from the actual organs' contours in the target image. These results can be regarded as encouraging step in confirming feasibility of conducting accurate registration of whole-body CT images using non-linear finite element models

without the necessity for time-consuming image segmentation when building patient-specific finite element meshes.

1 Introduction

Analysis of disease progression and response to therapy often involves quantitative comparison of two or more medical images of the whole body (or entire body segments) at different times or in different modalities [1]. However, before such comparison can be done, the images need to be aligned in a process known as image registration [2].

Numerous registration algorithms rely on image processing techniques have been proposed in the literature. Attempts have been made to use such algorithms for problems that involve rigid-body motions of articulated bones and non-linear deformations of soft tissues. They have proved to be successful only in the registration of selected body segments (e.g. neck images [3], [4]) and for limited range of rigid body motion and soft tissue (or soft organ) deformations. However, it has been recognised in the literature [5] [6] that registration of the whole body/torso images remains very challenging for the registration algorithms that are solely based on image processing techniques as it necessitates accounting for differences between images caused by complex rigid-body motions of articulated bones, non-linear motions of body organs and large deformation of soft tissues.

For registration problems involving large deformations of anatomical structures depicted in the image, many researchers advocate the use of patient-specific biomechanical models [7-10]. Our previous research in the development and application of algorithms for image registration in image-guided neurosurgery indicates that such algorithms can provide accurate and fast (within the real time constraints of image-guided neurosurgery) prediction of the deformation field within the organ (brain) undergoing surgery. In this study, we apply the experience and algorithms obtained in this research to the problem of registration of whole-body CT images. We use registration of the torso CT images as an example to demonstrate how we propose to solve the problem of efficient generation of computational grids (finite element meshes) for patient-specific models required for computation of deformations within the body and demonstrate the accuracy of such computation.

2 Methods

2.1 Patient-Specific Biomechanical Model

How to generate patient-specific biomechanical models quickly and reliably remains unresolved [11]. In this study, a set of methods are introduced to achieve this goal.

2.1.1 Generation of FEM Meshes

In this study, the Finite Element Method (FEM) is employed to compute the movement and deformation of the whole body. It is widely accepted that the accuracy of the FEM heavily depends on the quality of mesh generation [12]. In practice, the tetrahedral mesh is the most popular type of discretisation in computational biomechanics due to the availability of automatic mesh generation for arbitrary geometries [6]. However, the 4-noded tetrahedral element has an intrinsic drawback of volume locking when the materials are incompressible or nearly incompressible. Thus, we use the hexahedron element to discretise the whole-body geometry.

The whole-body CT scans were acquired from the Slicer Registration Library, Case #20: Intra-subject whole-body PET-CT (http://www.na-mic.org/Wiki/index.php/Projects:RegistrationLibrary:RegLib_C20b). This CT had slices with an acquisition matrix of $512 \times 512 \times 128$, yielding a spatial resolution of $0.98 \times 0.98 \times 5\,mm$. The whole-body geometry was built using the 3D SLICER (http://www.slicer.org/) and discretised by hexahedron elements using IA-FEMesh (http://www.ccad.uiowa.edu/MIMX/projects/IA-FEMesh) and Hypermesh (Altair Engineering, Troy, MI, USA).

2.1.2 Material Properties

Our previous studies show that the mechanical properties of the deformable continuum make little impact on the displacement results when the deformation problem is formulated as the pure displacement and displacement-zero traction problem [11] [13]. A FCM algorithm is adopted here to classify tissues and assign material properties automatically without the hard image segmentation for each organ [14]. The key step of the algorithm is to build the relationships between tissues and image intensity values. The FCM algorithm divides image intensity into different groups by computing the membership function between each pixel and all the specified cluster centres, and minimizing the objective function [14].

2.1.3 Loading

The patient-specific biomechanical model is driven by an imposed displacement, which is extracted from a pair of corresponding organs in whole-body images. We compare spines in these two whole-body CT scans because it is easy to distinguish the spine from surrounding soft tissues. Moreover, as a rigid structure, the displacement between two spines is calculated simply using the rigid registration, as show in Fig. 1. Considering the articulated structure, a whole spine is divided into separate vertebrae, and the rigid registration is applied to each pair of vertebra. Then, the deformation field between two spines is calculated by

$$D = \begin{pmatrix} x_f \\ y_f \\ z_f \end{pmatrix} - \begin{pmatrix} x_m \\ y_m \\ z_m \end{pmatrix} = (R - I) * \begin{pmatrix} x_m \\ y_m \\ z_m \end{pmatrix} + T \tag{1}$$

where D is the distance between two corresponding points in the source image and target image, $P_m(x_m, y_m, z_m)$ is a point in the moving (source) image, while $P_f(x_f, y_f, z_f)$ is the corresponding point in the fixed (target) image, R is the rotation transformation, T is the translation transformation and I is a diagonal matrix.

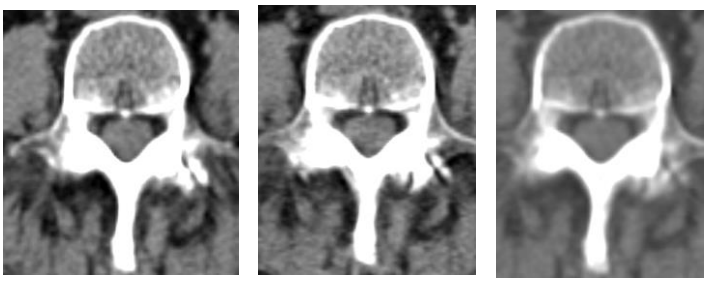

(a) (b) (c)

Fig. 1. Rigid registration of vertebra. (a) The vertebra from source images; (b) The vertebra from target images and (c) is the result of rigid registration for (a) and (b).

2.2 Numerical Solution

2.2.1 Total Lagrangian Explicit Dynamic Algorithm

A detailed description of TLED algorithm can be referred in [15]. This algorithm refers all variables to the original configuration, and the second Piola-Kirchoff stress and Green-Lagrangian strain are used. So, all the spatial derivatives with respect to spatial coordinates at original configuration can be pre-computed. Moreover, the explicit scheme uses the central difference method to

temporally discretise derivatives so that discretised equation can be solved by one step without any iteration.

2.2.2 Hourglass Control

The combination of hexahedron elements and one point integration leads to hourglass modes (zeros-energy modes). To address this problem, an effective method for the hourglass control was presented in [16]. Also, this method was used for hexahedron and quadrilateral elements with arbitrary geometry even undergoing large deformations [17].

3 Computation and Results

3.1 Meshes of the Whole-Body Geometry

The whole-body geometry is built from CT images and discretised by hexahedron elements, as shown in Fig. 2. The mesh quality is checked by two criteria, which are the Jacobian and warpage. In this study, the minimum Jacobian value is 0.35 and the maximum warpage value is 25. Total 51,479 elements and 55,944 nodes are generated in the whole-body volume.

3.2 Fuzzy C_Means Cluster Centres

Before applying the FCM algorithm to calculate the cluster centres, the number of clusters should be determined. There is no standard criterion to determine how many clusters are needed in a specific application, because the number of clusters depends on the image intensity depicted in an image. In this paper, tissues in whole-body images are roughly divided into 8 groups, and they are able to distinguish differences between different tissues. Table 1 shows the computed cluster centres, the corresponding tissues and mechanical properties.

3.3 Computed Results

To validate the feasibility of using patient-specific biomechanical models and the TLED algorithm for the prediction of whole-body deformation, all the algorithms were implemented by programming in Matlab. The computing computer is with a standard Intel® Core™ i7-3930K @3.20GHz CPU and windows 7 Enterprise with Service Pack 1.

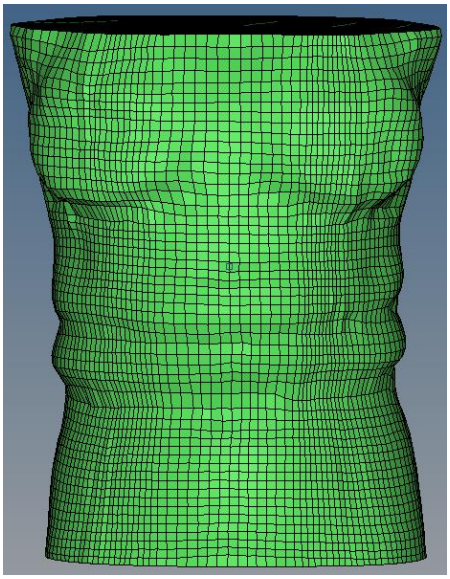

Fig. 2. Hexahedron meshes of the whole-body model. The discretised model consists of 51,479 hexahedron elements and 55,944 nodes

We verified the computation results by comparing the contours of abdomens, kidneys and lungs. This is because the comparison of abdominal contours can provide an overview of the accuracy of computation results, and the kidney and lung are the typical soft organs in the whole body. In addition, it is relative easy to get the contours for abdomens, kidneys and lungs from CT images.

Table 1. Cluster centres and mechanical properties

Cluster Centres	-813	-476	-108	-31	41	185	396	777
Tissues	Lung	Lung	Fat	Muscle	Ligament	Bone	Bone	Bone
Young's Modulus (kPa)	1.5	1.5	3.21	24.7	24.7	10^5	10^5	10^5
Poisson's Ratio	0.35	0.35	0. 48	0. 48	0.49	0.48	0. 48	0. 48
Mass Density (kg/m^3)	700	700	950	1059	1059	1817	1817	1817

(1) Comparison of Abdominal Contour

The comparison of abdominal contours is presented in Fig. 3. The abdominal contours are extracted from the target whole-body image (black solid line), the source whole-body image (blue dotted line) and the predicted image (red dashed line) which is warped by the computed deformation field, respectively. The difference between the black solid line and blue dotted line shows that the transformation from the source image to the target image is non-rigid. Also, it can be seen that the black solid line (target image) matches the red dashed line

(computed deformation) very well in the front and bio-lateral areas of the body. However, an apparent misalignment occurs on the right side of the back area of the body. The maximum misalignment is less than 0.01m, and the width of the body in *x* direction is 0.32m. Normalising the misalignment by the total width, the relative error is less than 3.2%. The misalignment might result from errors when performing rigid registration for vertebrae to calculate the deformation between two spines as the imposed displacement field.

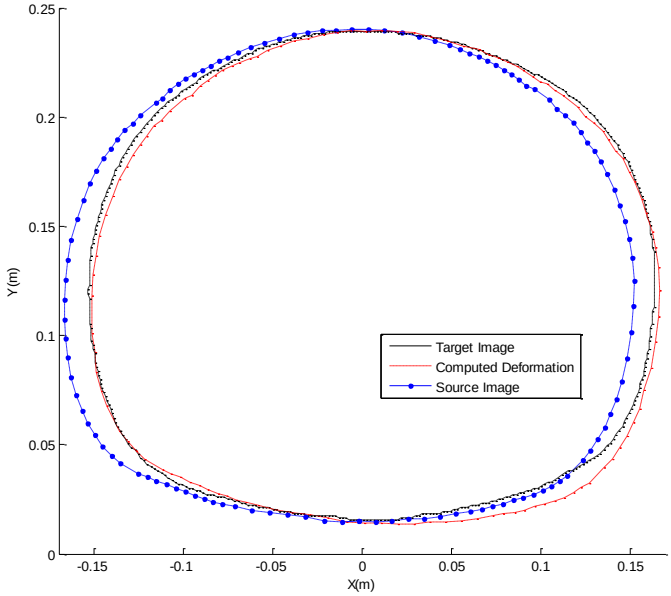

Fig. 3. Comparison of abdominal contours. The target image is represented by the black solid line, the computed deformation is represented by the red dashed line and the source image is represented by the blue dotted-solid line.

(2) Comparison of Kidney Contours

Fig. 4 shows the comparison of the cross section for kidneys. The red dashed line, the white solid line and the yellow dotted line represent the kidney contour in the deformed image, the target image and the source image, respectively. The difference between source image and target image is very big and nonlinear, while the use of patient-specific biomechanical model successfully predicts the transformation from the source image to the target image.

(3) Comparison of Lung Contours

In comparison with the abdomen and kidney, the structure of the lung is more complex. Fig. 5 shows that the source image (yellow dotted line) is very different from the target image (white solid line). However, after applying the computed deformation field to warp the source image, the predicted image (red

dashed line) can align to the target image. There may be two reasons for the misalignment. Firstly, the errors from rigid registration for vertebrae will influence the result of deformation prediction, as discussed previously. Secondly, the relative large space resolution in perpendicular direction and the quick variation of lung from one slice to another may cause the warped slice from the source image does not match exactly to the corresponding slice in the target image.

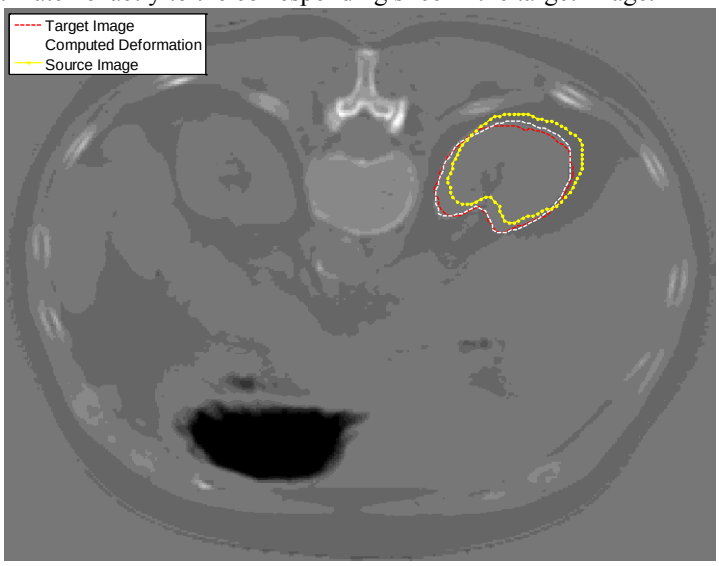

Fig. 4. Comparison of contours for the kidney. The red dashed line is extracted from the target image, the white solid line is extracted from the computed deformation and the yellow dotted line is extracted from the source image.

4 Conclusions

Registration of whole-body CT scans is extremely challenging because non-linear deformations of body organs and articulated skeletal motions are involved and, accordingly, the differences between the source image and the target image are very large. Thus, a comprehensive patient-specific non-linear finite element model and the TLED algorithm are used to predict the deformation of body organs and soft tissues.

Due to the efficiency of using hexahedron elements for the computation of incompressible biological tissues, the whole-body geometry is discretised by hexahedron (8-noded brick) elements. Accordingly, an efficient hourglass control algorithm is employed to overcome the intrinsic zero energy mode of under-integrated hexahedron elements. Moreover, the assignment of material properties is facilitated using the FCM algorithm for tissues classification without the hard image segmentation.

To drive the patient-specific model, an imposed displacement which is obtained using the rigid registration for corresponding vertebrae is applied on the spine.

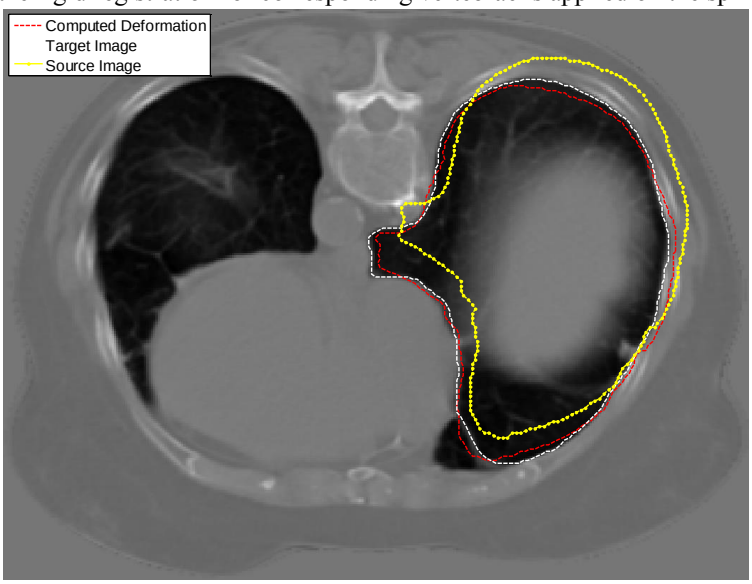

Fig. 5. Comparison of contours for the lung. The red dashed line represents the computed deformation, the white solid line represents the target image and the yellow dotted line represents the source image.

To the authors' knowledge, it is the first time to use a patient-specific non-linear finite element model to conduct the whole-body image registration. In this work, we used a patient-specific torso example to verify the proposed algorithms, and the results confirmed that our methods facilitate the accuracy of predicting the organs deformations. In the next step, we will analyse more torso examples to demonstrate the quantitative accuracy of our methods for the whole-body CT image registration.

Acknowledgments The first author is a recipient of the SIRF scholarship and acknowledges the financial support of the University of Western Australia. The financial support of National Health and Medical Research Council (Grant No. APP1006031) and Australian Research Council (Discovery Grants No. DP1092893 and DP120100402) is gratefully acknowledged. This investigation was also supported in part by NIH grants R01 EB008015 and R01 LM010033, and by a research grant from the Children's Hospital Boston Translational Research Program. In addition, the authors also gratefully acknowledge the financial support of National Centre for Image Guided Therapy (NIH U41RR019703) and the National Alliance for Medical Image Computing (NAMIC), funded by the National Institutes of Health through the NIH Roadmap for Medical Research, Grant U54 EB005149. Information on the National Centres for Biomedical Computing can be obtained from http://nihroadmap.nih.gov/bioinformatics.

10

References

1. Makela T, Clarysse P, Sipila O, Pauna N, Pham QC, Katila T, Magnin IE: A review of cardiac image registration methods. IEEE Trans Med Imaging 2002, 21(9):1011-1021.
2. Hill DL, Batchelor PG, Holden M, Hawkes DJ: Medical image registration. Phys Med Biol 2001, 46(3):R1-45.
3. Little JA, Hill DLG, Hawkes DJ: Deformations incorporating rigid structures. Comput Vis Image Und 1997, 66(2):223-232.
4. d'Aische AD, De Craene M, Geets X, Gregoire V, Macq B, Warfield SK: Efficient multi-modal dense field non-rigid registration: alignment of histological and section images. Med Image Anal 2005, 9(6):538-546.
5. Li X, Yankeelov TE, Peterson TE, Gore JC, Dawant BM: Automatic nonrigid registration of whole body CT mice images. Med Phys 2008, 35(4):1507-1520.
6. Wittek A, Miller K, Kikinis R, Warfield SK: Patient-specific model of brain deformation: application to medical image registration. J Biomech 2007, 40(4):919-929.
7. Hagemann A, Rohr K, Stiehl HS, Spetzger U, Gilsbach JM: Biomechanical modeling of the human head for physically based, nonrigid image registration. Ieee T Med Imaging 1999, 18(10):875-884.
8. Otoole RV, Jaramaz B, Digioia AM, Visnic CD, Reid RH: Biomechanics for Preoperative Planning and Surgical Simulations in Orthopedics. Computers in biology and medicine 1995, 25(2):183-191.
9. Rohlfing T, Maurer CR, O'Dell WG, Zhong JH: Modeling liver motion and deformation during the respiratory cycle using intensity-based nonrigid registration of gated MR images. Med Phys 2004, 31(3):427-432.
10. Snedeker JG, Wirth SH, Espinosa N: Biomechanics of the normal and arthritic ankle joint. Foot and ankle clinics 2012, 17(4):517-528.
11. Miller K, Wittek A, Joldes G: Biomechanical Modeling of the Brain for Computer-Assisted Neurosurgery. Biol Med Phys Biomed 2011:111-136.
12. Ramos A, Simoes JA: Tetrahedral versus hexahedral finite elements in numerical modelling of the proximal femur. Med Eng Phys 2006, 28(9):916-924.
13. Wittek A, Hawkins T, Miller K: On the unimportance of constitutive models in computing brain deformation for image-guided surgery. Biomech Model Mechan 2009, 8(1):77-84.
14. Zhang JY, Joldes GR, Wittek A, Miller K: Patient-specific computational biomechanics of the brain without segmentation and meshing. Int J Numer Meth Bio 2013, 29(2):293-308.
15. Miller K, Joldes G, Lance D, Wittek A: Total Lagrangian explicit dynamics finite element algorithm for computing soft tissue deformation. Commun Numer Meth En 2007, 23(2):121-134.
16. Flanagan DP, Belytschko T: A Uniform Strain Hexahedron and Quadrilateral with Orthogonal Hourglass Control. Int J Numer Meth Eng 1981, 17(5):679-706.
17. Joldes GR, Wittek A, Miller K: An efficient hourglass control implementation for the uniform strain hexahedron using the Total Lagrangian formulation. Commun Numer Meth En 2008, 24(11):1315-1323.